Fabrication and characterization of Se₆₆S_{44-x}As_x thin films chalcogenide

D. M. A. Latiff, B. A. Ahmed, S. M. Ali, K. A. Jasim* Department of Physics, College of Education for Pure Sciences ibn Al-Haitham, University of Baghdad, Iraq

In this paper, the effect of sulfur substitution by arsenic on the structural, optical properties of thin films of the trivalent chalcogenide Se₆₆S_{44-x}As_x at different concentrations (where x = 0, 8, 16, and 24 at %) was studied. Thin films with a thickness of (300±10 nm) were prepared using thermal evaporation of bulk samples. Structural examinations were performed using XRD and AFM techniques. All the studied film samples were amorphous in structure and the intensity of the crystalline parts was high in the range of 10-40. Also, in Atomic Force Microscopy (AFM). It was found that increasing the concentration of arsenic affects the structural parameters such as surface roughness, particle density, and average grain size. As the arsenic element increased by 0.24, the grains became more regular, and the particle density increased. UV-Vis measurements reveal that the prepared films' absorption in the spectral wavelength range from 200 to 1100 nm. It was found that increasing the arsenic content led to a change in the absorbance of the films. The optical energy gap of Se₆₆S_{44-x}As_x thin films was determined and it was found that increasing arsenic content affected the energy gap differently as it changed within the range (2.35-2.19 eV). The energy gap increased at concentrations of (8, 16%) while the energy gap decreased at concentrations of 24%.

(Received March 25, 2025; Accepted June 10, 2025)

Keywords: Alloy, Thermal evaporation technique, Thin films, XRD, AFM, Optical properties

1. Introduction

In general, amorphous materials are disordered systems. There are two types of disorder: configurational disorder, which arises in binary crystalline alloys, and the topological disorder, which arises in the liquids. Amorphous solids may encounter topological problems [1]. However, it exhibits short-range order because of the chemical bonding of the constituent atoms. due to spatial changes in bond angles, bond lengths, and dihedral angles, tail states arise in the area of band gap, that is, above the valence band edge and below the conduction band edge [2, 3]. The band gap is known as the mobility gap, while the borders of the valence band and conduction band are known as the mobility edges. Dissocialized and the localized states are separated by these edges [4]. The states above the conduction edge and below the valence edge are called extended states, while the levels between the two edges are called localized states. This can be seen in Figure (1). Anderson localization is the term used to describe the abnormality that creates these boundaries. Since there is no translational order in an amorphous lattice, the Bloch theory of crystalline solids cannot be applied; however, the electronic amorphous semiconductors properties can be understood by applying the density functional methodology, Hartree-Fock approximation, or tight-binding model [5].

The structure of actual samples is different from that of an ideal amorphous network, that is, the constituent atoms deviate from natural coordination according to the 8-N rule [6], even though the above is based on a continuous random network. where N is the periodic table's pertinent column number. In this study, only the elements listed in the periodic table columns IV-VI of the periodic table were considered. Z (valence) = N if N < 4 is an additional rule that can be applied. For instance, amorphous silicon has tetragonal coordination by nature, yet certain silicon atoms are triply coordinated.

_

^{*} Corresponding author: kareem.a.j@ihcoedu.uobaghdad.edu.iq https://doi.org/10.15251/CL.2025.226.521

Selenium atoms are singly and triply coordinated and other coordination is structural defects because amorphous selenium naturally shows divalent coordination, which is defects such as band tails and structural defects. Which affects the optical, electrical and structural properties of amorphous semiconductors and chalcogenides, which are a kind of amorphous semiconductors. To understand these cases, it is important to clarify their optical properties and structure [7].

Chalcogenides are chemical compounds that contain at least one chalcogenide anion and an electropositive element. Although all elements in group 16 of the periodic table are referred to as chalcogenides, sulfides, selenides, tellurides, and polyiodides are more often referred to as chalcogenides than oxides [8]. Chalcogenides are found in many mineral ores. In xerography, light-conducting chalcogenide glasses are used. Chalcogenides are also the basis for many colors and catalysts.

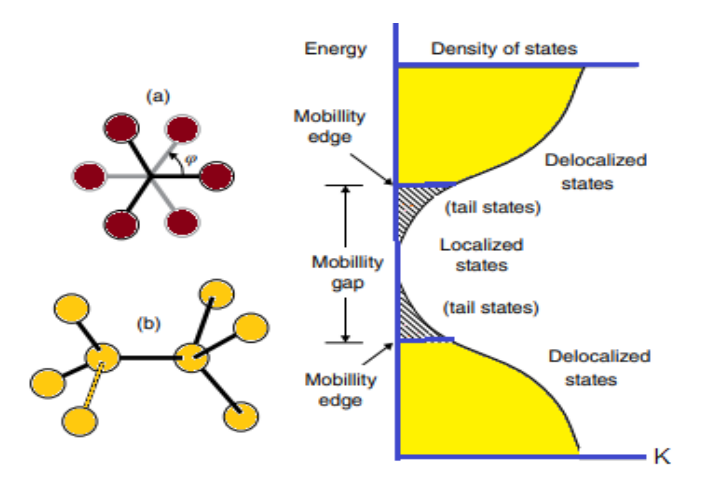


Fig. 1. Schematic diagram showing the state density in an amorphous semiconductor.

Chalcogenide semiconductors are sensitive materials for electron beam recording [9-12] and photo conversion (photo-optical dimming, photo refraction) [10-12] and as photoresists sensitive in the visible and ultraviolet regions [13]. Various carriers and methods for recording optical information have been developed and studied. Chalcogenide semiconductors of the Se.S.As system are auspicious materials for recording optical information. Thin films of As₂S₃, as photoresists for X-ray photolithography, have been studied in the work [14].

The phenomenon of light-induced changes and electron beam dissolution a large range rate of amorphous chalcogenide films has been the basis for the intensive development of a new class of inorganic resists [15, 16]. As–S, As–Se amorphous films have recently been used as promising materials for photolithography with high resolution and photosensitivity in the visible spectrum. Amorphous alloys have a typical XRD pattern because the regularity degree of atomic positions in these systems is very small. When examined in an XRD instrument, these alloys produce broad diffuse halos. It is necessary to distinguish between the parts' crystalline and amorphous components. These calculated results are compared with outcomes determined by the stable software of the X-ray equipment's stable software and the part that is amorphous determined by differential scanning calorimetry (DSC). The evaluation of XRD is often time-consuming and difficult [17]. In this paper, we will prepare chalcogenide alloys Se₆₆S_{44-x}As_x with different element concentrations x= 0, 8, 16, and 24, to determine the effect of partial substitution elements on the structural and optical properties.

2. Experimental work

Four thin films of $Se_{66}S_{44-x}As_x$ alloy (x = 0, 8, 16, and 24) with different concentrations of high-purity (99.999%) selenium, sulfur, and Arsenic elemental powders were prepared by the

thermal evaporation technique after weighing the samples according to their atomic weight ratios. The powder from each sample was placed in vacuum ampules at a pressure of 10⁻⁵ Torr. The ampoules were tightly sealed and placed in an oven and they were heated so the oven temperature was gradually raised to the melting point at a rate of 5 °C/min. The ampoules remained in the oven at a high temperature of 600 °C for 4 hours, and then they were heated to 950 °C for 12 hours. The ampoules were taken out of the oven and quickly placed in ice water, then they were broken and the alloys were extracted. The resulting samples were then ground to powder using a mortar and pestle. The sample powders were pressed and made into tablets (2 mm thick and 15 mm in diameter). For this purpose, a hydraulic press was used under a pressure of seven tons per cm². The samples were placed in a molybdenum boat in a vacuum evaporator at 10⁻⁵ Torr, an electric current was passed through the boat gradually to prevent the boat from breaking, and when the temperature of the boat reached the required temperature, the deposition process began at a constant deposition rate (27±2) nm/s). Before measurements, the thin films were taken out of the coating machinery and placed in vacuum dryers. Each sample was made with consistent pressure, substrate temperature, thickness, and deposit rate; thin films with a thickness of (300±10 nm) were obtained in this way. The structural state of the films was examined using an X-ray diffraction apparatus (Philips 1710 type with copper as target and nickel as filter; $\lambda = 1.5418 \text{ Å}$). Structural morphology was also analyzed using atomic force microscopy (AFM). A dual-beam UV-Vis spectrometer (Shimadzu 2101) was used to measure the absorbance of the prepared films in the spectral wavelength range of 300 to 1100 nm.

3. Result and discussion

3.1. XRD analysis

In this work, the XRD patterns of $Se_{66}S_{44-x}As_x$ with different element concentrations x=0, 8, 16, and 24 were studied using an X-ray diffractometer. The amorphous nature can be seen by the graphical analysis of the system's XRD pattern [18]. The X-ray diffraction pattern records the intensity as a function of the 2θ .

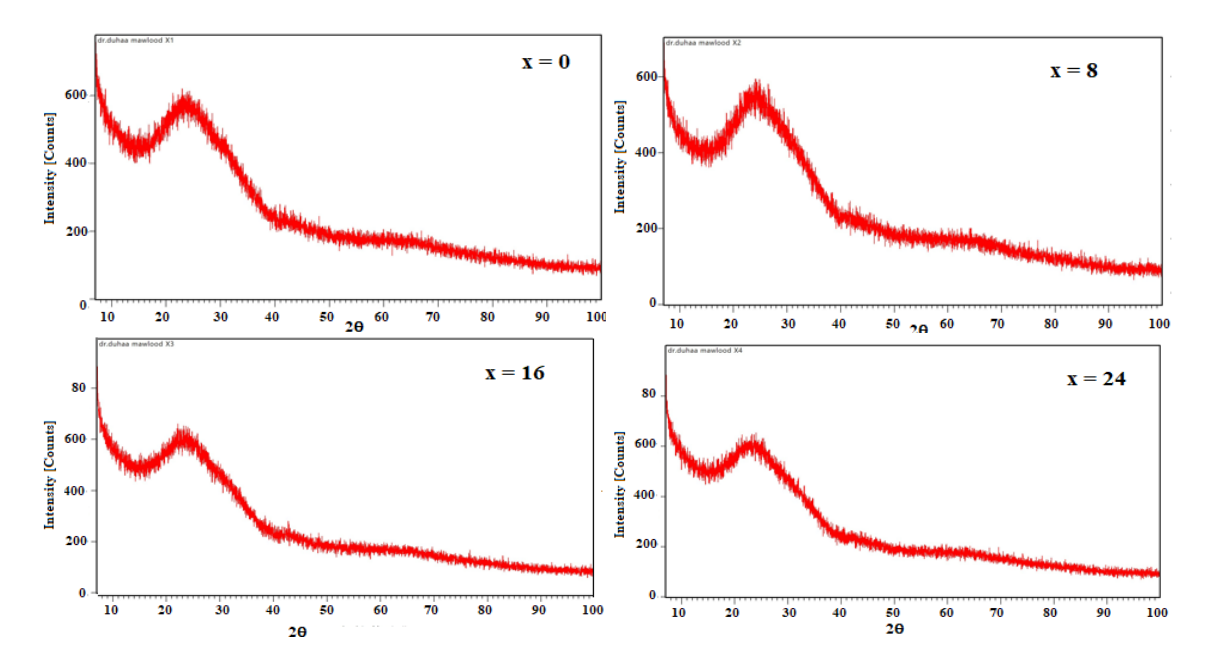


Fig. 2. XRD patterns of $Se_{66}S_{44.x}As_x$ thin films (x = 0, 8, 16, and 24,) with different concentrations.

The intensity was measured from 200 to 600. The diffraction lines absence in the X-ray patterns indicates that all films have amorphous structures, the amorphous matrix scatters X-ray photons within this range. It is evident from the diffraction plots that there is no clear pattern as to

whether crystallinity is generally higher or lower for the film-form samples [19, 20]. All the alloys under investigation were amorphous in composition and the intensity of the crystalline parts was high in the range of 10-40, while for angles above that it was negligibly small. Integrating radially along the x-axis gives the radial peak widths for the equatorial reflections (15 - 35) when x = 0 and the meridional reflections (10 - 40), (5 - 30) and (15 - 40) when x = 8, 16 and 24 respectively. This behavior is consistent with the four samples for different concentrations of as, as shown in Figure. 2.

3.2. Atomic Force Microscopy (AFM)

Structural morphology was also analyzed using atomic force microscopy (AFM). Figure (3) shows the images taken by atomic force microscopy of the four samples. It was found that increasing arsenic concentration affects structural parameters such as surface roughness and average grain size. This figure shows the variation in the sizes of the particles when the concentrations of the elements in the manufactured films change.

Different as thin films were imaged by atomic force microscopy for freshly cleaned samples (Fig. 3). Increasing the Arsenic concentration from 0 to 8 in the first and second samples leads to an increase in the density of particles on the surface. The lateral sizes of the particles varied from one image to another due to the difference in top shape. However, the height was found to vary from 4 to 82 nm.

When the Arsenic element was increased by 0.24, the grains were more regular, in addition to the increased particle density [21]. The particle density was very high compared to the As-free sample. When the film particles were deposited on this substrate, the surface responded to the adhesion of the particles and thus the particles adhered to the surface [22]. This is the reason for the increased particle density on the substrate [23].

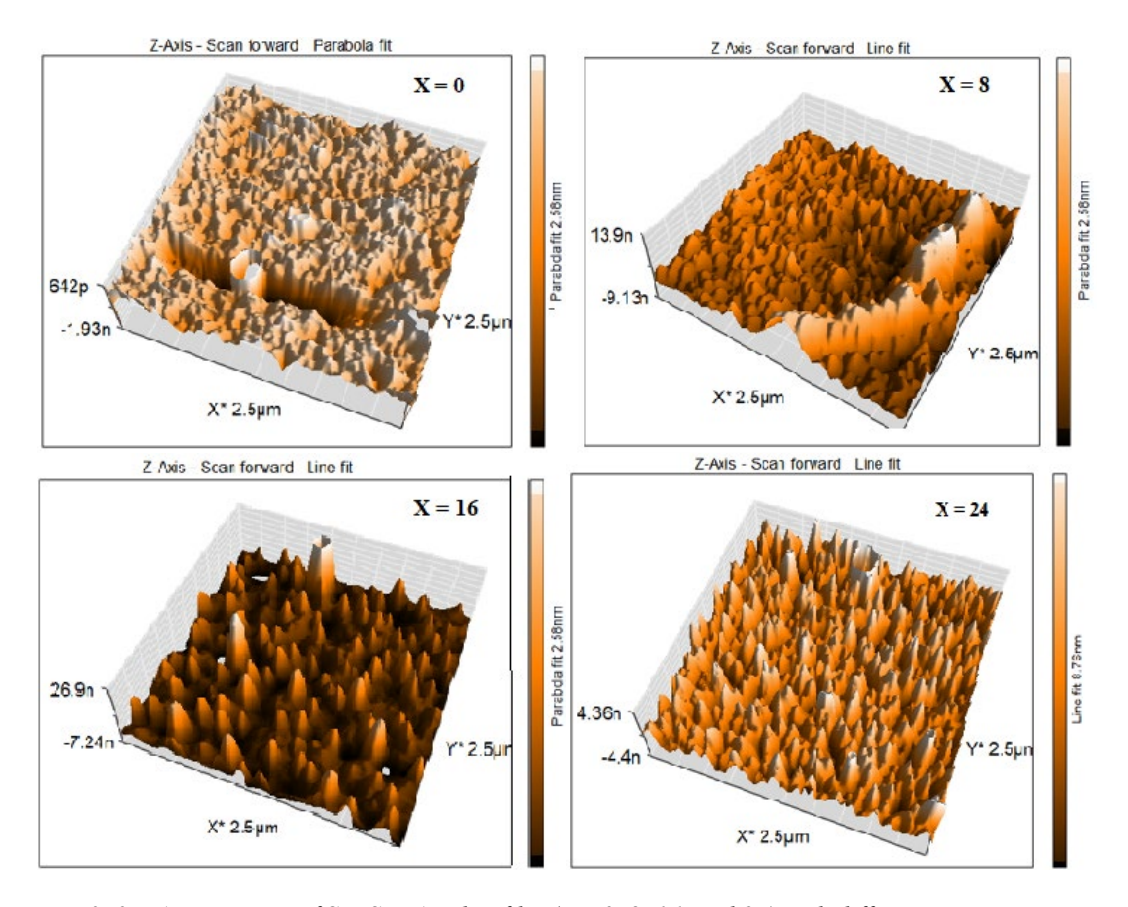


Fig. 3. 3D AFM images of $Se_{66}S_{44-x}As_x$ thin film (x = 0, 8, 16, and 24) with different concentrations.

3.3. Optical properties

The optical properties of $Se_{66}S_{44-x}As_x$ films with different ratios (x = 0, 8, 16, and 24) were studied using dual-beam UV-Vis spectroscopy to measure the absorption and bandgap of the films in a spectral wavelength range of 300 to 1100 nm. The forbidden energy gap for the allowed direct electronic transitions was calculated, and the absorption and reflectivity coefficients were calculated.

The study of the optical properties of semiconductors is of great importance for their applications in many electronic devices because it provides a lot of information about the electronic transitions and their type that occur inside the material in addition to the structure of the energy bands and it also describes the distinctive properties that determine the interaction of light with the material [24, 25].

The absorbance spectra were measured within the wave length range (300-1100 nm) for all $Se_{66}S_{44-x}As_x$ films with different ratios (x = 0, 8, 16, and 24). Figure (4) shows the change in the absorption spectrum as a function of wavelength, where the absorption of all films is at its maximum at the fundamental absorption edge (short wavelengths), i.e. the prepared films are characterized by high absorption at short wavelengths and then decreases with increasing wavelength, that the incident photon was unable to excite electrons and transfer electron from the valence band to conduction band because the incident photon energy is less than the energy gap value of the semiconductor. Thus, the absorption decreases with increase wavelength [26,27]. It was noted that absorption falls within the visible region (between 300 to 600), This means physically, can be used in solar cell applications [28,29].

It was also noted from Figure 4 that absorption increases with increasing arsenic concentration because Arsenic has a radius $(1.33 \times 10^{-10} \text{ m})$ larger than selenium $(1.22 \times 10^{-10} \text{ m})$ and a difference in the oxidation states of each of them (Se^{-2, 4, 6} and As^{-3, 3,5}), which made the process of absorbing the incident photon directly proportional to the increase in the concentration of As [30, 31].

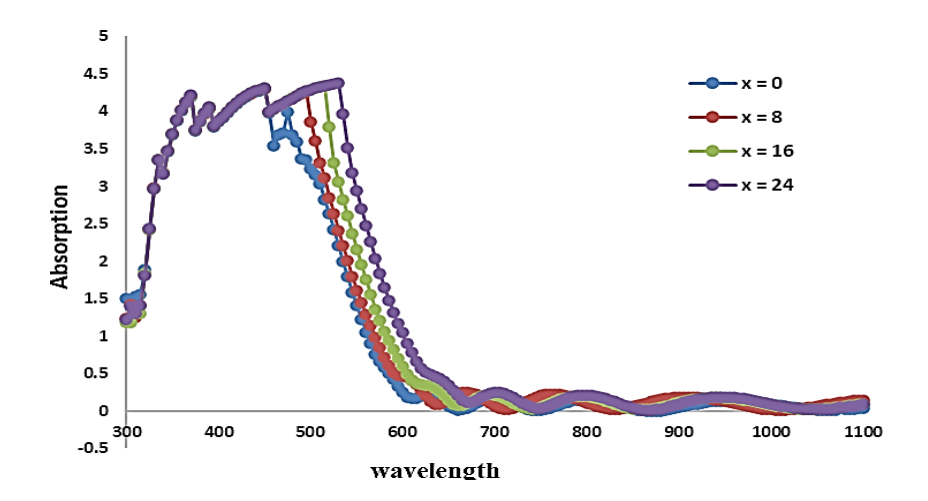


Fig. 4. Optical absorption of $Se_{66}S_{44-x}As_x$ thin film (x = 0, 8, 16, and 24) with different concentrations.

The optical energy gap for the electronic transitions of $Se_{66}S_{44-x}As_x$ films with different ratios (x = 0, 8, 16, and 24was calculated using the relation [32]:

$$\alpha hv = B_h (hv - E_g^{opt})^r$$

where B_h : A constant that depends on the nature of the material, r: An exponential factor that determines the type of transition, E_g^{opt} represents the optical energy gap in units (eV) and hv: The incident photon energy in units.

By drawing the linear relation between $(\alpha hv)^2$ and the incident energy of photon (hv) and extending the curve straight part to cut the photon energy axis in the point $(\Box hv)^2$ at the point = 0

and touching the curve from the top of the curve since the relation (1) is satisfied, that is, the cutting point represents the optical energy gap value (E_g^{opt}) as shown in Figure 5.

From Figure 5, it is noted that the partial replacement of selenium with arsenic for $Se_{66}S_{44}$. $_xAs_x$ films led to a decrease in the value of the optical energy gap for all arsenic concentrations. This means that the replacement with arsenic led to a shift of the absorption edge towards lower energies. This decrease can be explained as a result of Bureshtain-Moss Shift, because the levels close to the conduction band are almost empty of electrons, so the electrons need less energy to move [33-36].

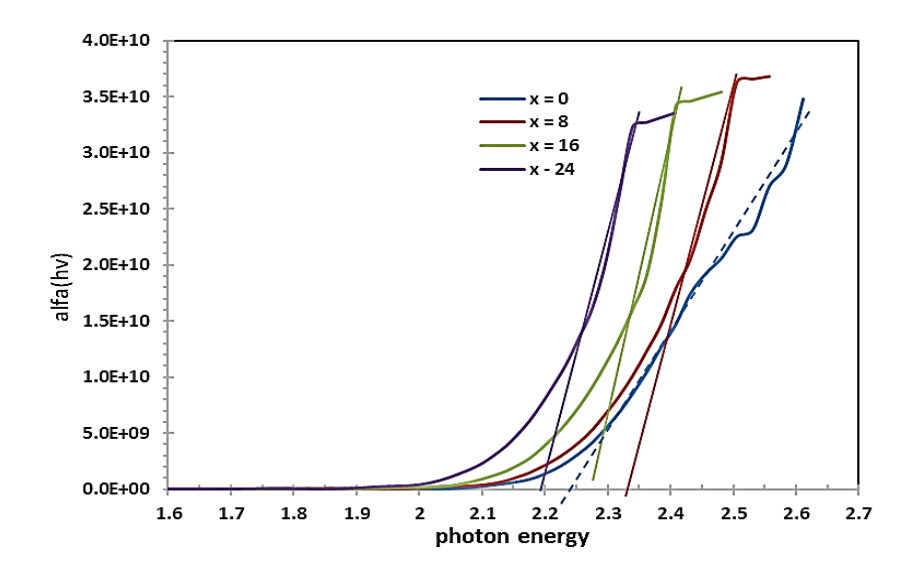


Fig. 5. $(\alpha h v)^2$ versus photon energy gap of $Se_{66}S_{44-x}As_x$ thin films continuously.

4. Conclusions

Amorphous Se₆₆S_{44-x}As_x thin films with different element concentrations x=0, 8, 16 and 24 were prepared as thin films by the thermal evaporation technique under optimum conditions. The material exhibits highly random structural behaviors with peaks appearing at almost the same positions in all samples with little variation due to the effect of minimal arsenic concentrations, but with some distortions due to stress and deformation effects resulting from cold working or annealing. The surfaces of the samples were studied using AFM and XRD, and it was found that the surfaces changed with the arsenic concentration. The optical properties were studied and it was observed that the absorption edge shifts towards lower energies as the arsenic concentration increases, in addition to the decrease in the energy gap.

References

[1]Shore, K. A. (2014), Contemporary Physics, 55(4), 337-337; https://doi.org/10.1080/00107514.2014.933254

- [2] Mohammed, J. S., Nsaif, F. K., Jawad, Y. M., Jasim, K. A., Al Dulaimi, A. H. (2023), Chalcogenide Letters, 20(7), 449-458; https://doi.org/10.15251/CL.2023.207.449
- [3] Aqeel N. Abdulateef, Ahlam Alsudani, Riyadh Kamil Chillab, Kareem A. Jasim, Auday H. Shaban, Journal of Green Engineering (JGE), 10.9: 5487-5503,2020.
- [4] Chillab, R. K., Jahil, S. S., Wadi, K. M., Jasim, K. A., Shaban, A. H. (2021), Key Engineering Materials, 900, 163-171; https://doi.org/10.4028/www.scientific.net/KEM.900.163
- [5] Ahmed, B. A., Mohammed, J. S., Fadhil, R. N., Jasim, K. A., Shaban, A. H., Al Dulaimi, A. H. (2022), Chalcogenide Letters, 19(4), 301-308; https://doi.org/10.15251/CL.2022.194.301

- [6] Khudhair, N. H., Jasim, K. A. (2023), Ibn AL-Haitham Journal For Pure and Applied Sciences, 36(1), 149-157; https://doi.org/10.30526/36.1.2892
- [7] A. Chirita, V. Prilepov, Chalcogenide Letters Vol. 19, No. 6, June 2022, p. 439 445 https://doi.org/10.15251/CL.2022.196.439
- [8] M. Iovu, S. Sergeev, O. Iaseniuc, Optoelectron. Adv. Mat. 12(7-8), 377 (2018).
- [9] O. Iaseniuc, M. Enachescu, D. Dinescu, M. Iovu, S. Sergheev, J. Optoelectron. Adv. M. 18(1-2), 34 (2016).
- [10] S. Sergeev, M. Iovu, A. Meshalkin, Chalcogenide Letters 17(1), 25 (2020); https://doi.org/10.15251/CL.2020.171.25
- [11] Nawal Hassan khudhair, Kareem Ali Jasim, AIP Conf. Proc. 2769, 020062-1-020062-7; https://doi.org/10.1063/5.0129373
- [12] Nawal Hassan khudhair, Kareem Ali Jasim, AIP Conf. Proc. 2769, 020056-1-020056-7; https://doi.org/10.1063/5.0129550
- [13] Sharma, N., Sharma, S., Sarin, A., Kumar, R. (2016), Optical Materials, 51, 56-61. https://doi.org/10.1016/j.optmat.2015.11.021
- [14] Tripathi, S., & Kumar, A. (1988), Journal of Non-Crystalline Solids, 104(2-3), 229-236; https://doi.org/10.1016/0022-3093(88)90393-6
- [15] C. Meneghini, A. Villeneuve, J. Opt. Soc. Am. B 15(12), 2946-2950 (1998); https://doi.org/10.1364/JOSAB.15.002946
- [16] J. Z. Liu, P. C. Taylor, Phys. Rev. Lett. 59(17), 1938-1941 (1987).
- [17] G. Kőrösy, K. Tomolya, D. Janovszky, J. Sólyom, Materials Science Forum Vol. 729 (2013) pp 419-423; https://doi.org/10.4028/www.scientific.net/MSF.729.419
- [18] Thouless, D. J. (1980), The international series of monographs on physics. Science, 207(4436), 1196-1197; https://doi.org/10.1126/science.207.4436.1196-b
- [19] C. Mwolfe, N. Holouyak, G.B. Stillmau, Physical Properties of Semiconductor, Printice Hall, New York (1989).
- [20] S.O. Kasap, Principles of Electronic Materials and Devices, 2nd, Mc Graw-Hill, New York, (2002).
- [21] J. Tauc, J. of Non Non-Crystalline Solid, V. 8, No.10, (1972), P.519; https://doi.org/10.1016/0022-3093(72)90194-9
- [22] O. Stenz-el, The Physics of Thin Film Optical Spectra, An Introduction, Winz erlaer Str.Winz 10, 07745Jena, Germany, (2005).
- [23] Prasad, C. J. Zha, R. P. Wang, A. Smith, S. Madden, B. Luther-Davies, "Opt. Express 16(4), 2804-2815 (2008); https://doi.org/10.1364/OE.16.002804
- [24] Ram, I. S., Kumar, S., Singh, R. K., Singh, P., Singh, K. (2015), AIP Advances, 5(8), 087164; https://doi.org/10.1063/1.4929577
- [25] Ram, I. S., Kumar, S., Singh, R. K., Singh, P., Singh, K. (2015), AIP Advances, 5(8), 087164; https://doi.org/10.1063/1.4929577
- [26] Mobarak, M., Shaban, H., Elhady, A. (2008), Materials Chemistry and Physics, 109(2-3), 287-290; https://doi.org/10.1016/j.matchemphys.2007.11.025
- [27] Sikka, P., Ferdinand, K. V., Jagadish, C., Mathur, P. C. (1985), Journal of Materials Science, 20(1), 246-254;
- https://doi.org/10.1007/BF00555918
- [28] Paul, D. K., Mitra, S. S. (1973), Physical Review Letters, 31(16), 1000-1003; https://doi.org/10.1103/PhysRevLett.31.1000
- [29] Ibrahim, Z.H., Ibrahim, S.A., Shaban, A.H., Jasim, K.A., Mohammed, M.K., Baghdad Iraq with Aid of GIS Techniques, Energy Procedia, 2017, 119, pp. 709-717; https://doi.org/10.1016/j.egypro.2017.07.098
- [30] Jasim, K.A., Alwan, T.J., Al-Lamy, H.K., Mansour, H.L, Journal of Superconductivity and Novel Magnetism, 2011, 24(6), pp. 1963-1966;

https://doi.org/10.1007/s10948-011-1153-1

- [31] R. P. Wang, A. V. Rode, D. Y. Choi, B. Luther-Davies, J. Appl. Phys. 103(8), 083537 (2008); https://doi.org/10.1063/1.2909883
- [32] L. Petit, N. Carlie, R. Villeneuve, J. Massera, M. Couzi, A. Humeau, G. Boudebs, K. Richardson, J. Non-Cryst. Solids 352(50-51), 5413-5420 (2006); https://doi.org/10.1016/j.jnoncrysol.2006.08.040
- [33] S. Lorente, A. Bejan, and J. L. Niu, J. Heat Mass Transf., vol. 81, pp. 283-288, 2015; https://doi.org/10.1016/j.ijheatmasstransfer.2014.09.077
- [34] H. Wang, A. K. Prasad, S. G. Advani, Int. J. Hydrogen Energy, vol. 37, no. 19, pp. 14292-14299, Oct. 2012; https://doi.org/10.1016/j.ijhydene.2012.07.016
- [35] 35. Latif, D. M. A., Mahdi, H. A., Nsaif, F. K., & Abd, A. N., NeuroQuantology, 2021, 18(5), 83-8; https://doi.org/10.21608/ijmsat.2022.231331
- [36] 36. Abd, A. N., Al Hussan, S. M., & Latif, D. M. A. Plant Archives, 2020, 20(1), 1-5.